

Nonlinear dynamic analysis of RC frames using cyclic moment-curvature relation

Hyo-Gyoung Kwak[†], Sun-Pil Kim[‡] and Ji-Eun Kim[‡]

Department of Civil and Environmental Engineering, Korea Advanced Institute of Science and Technology, 373-1 Gusong-dong, Yuseong-gu, Daejeon 305-701, Korea

(Received January 17, 2003, Accepted November 17, 2003)

Abstract. Nonlinear dynamic analysis of a reinforced concrete (RC) frame under earthquake loading is performed in this paper on the basis of a hysteretic moment-curvature relation. Unlike previous analytical moment-curvature relations which take into account the flexural deformation only with the perfect-bond assumption, by introducing an equivalent flexural stiffness, the proposed relation considers the rigid-body-motion due to anchorage slip at the fixed end, which accounts for more than 50% of the total deformation. The advantage of the proposed relation, compared with both the layered section approach and the multi-component model, may be the ease of its application to a complex structure composed of many elements and on the reduction in calculation time and memory space. Describing the structural response more exactly becomes possible through the use of curved unloading and reloading branches inferred from the stress-strain relation of steel and consideration of the pinching effect caused by axial force. Finally, the applicability of the proposed model to the nonlinear dynamic analysis of RC structures is established through correlation studies between analytical and experimental results.

Key words: RC frame; earthquake loading; anchorage slip; pinching effect; Bauschinger effect; moment-curvature relationship.

1. Introduction

Reinforced concrete (RC) frame structures in regions of high seismic risk generally experience many earthquakes, developing inelastic deformations when subjected to strong ones. Present seismic design recommendations (FEMA-273 1997, Seacoc 1999) also intend that structures respond elastically only to small magnitude earthquakes, but should be expected to experience different degrees of damage during moderate and strong ground motions. Accordingly, a complete assessment of the seismic resistant design of RC frame structures often requires a nonlinear dynamic analysis. The nonlinear dynamic responses of RC frame structures under earthquake excitations are usually developed at certain critical regions, which are often located at points of maximum internal forces such as the beam-column joints. This means that an accurate numerical model able to simulate the hysteretic behavior of RC columns and beams is necessary in order to exactly predict the nonlinear response of the frame structures. Since earthquake-induced energy is dissipated through the

[†] Associate Professor

[‡] Graduate Student

formation of plastic hinges in the beams and columns, the determination of influence factors that affect to the nonlinear response at a joint is an essential step in the construction of a numerical model. Typically, initial stiffness, bond-slip, anchorage slip, shear span ratio, and axial force effects are some of the influence factors that must be included in the numerical model because the major sources of deformation in RC frame structures are the flexural rotation, shear deformation including shear sliding, and the bond-slip. The hysteretic load-deformation behavior of a frame member arises from a combination of these deformation mechanisms.

Many analytical models have been proposed to date for the nonlinear analysis of RC frame structures; these range from very refined and complex local models to simplified global models (D'Ambrisi and Filippou 1997, Kwak and Kim 2001, Taucer *et al.* 1991). In the case of frame structures, a numerical model based on the moment-curvature relation is often used. Since the first introduction of bilinear moment-curvature relationship by Clough and Johnson (1966), many mechanical models for the hysteretic moment-curvature relationship have been proposed to analyze the behavior of RC beams subjected to cyclic loading. Such models include cyclic stiffness degradation (Chung *et al.* 1998, Dowell *et al.* 1998, Takeda *et al.* 1970). Also, further modifications to take into account the pinching effect due to shear force and strength degradation after yielding of steel have been introduced (Roufaiel and Meyer 1987). In addition, by using the bilinear, instead of a trilinear, hysteretic curve, a more simplified model has been proposed. Recently, the inclusion of the axial load effect has received the attention of many researchers (Assa and Nishiyama 1998, Watson and Park 1994). Nevertheless, these models still have limitations in simulating exact structural behavior by excluding bond-slip and the Bauschinger effect.

In this paper, a curved hysteretic moment-curvature relationship is introduced. Unlike previously proposed models, bond slip effects are taken into account by defining the initial loading branch on the basis of the monotonic moment-curvature relationship introduced in previous paper (Kwak and Kim 2002). The following curved hysteretic unloading and reloading branches are defined; the fixed-end rotation at the beam-column joint interface and the pinching effect caused by the applied shear force are also taken into consideration. The validity of the proposed model is established by comparing the analytical predictions with results from experimental and previous analytical studies. A correlation study between analytical results and experimental values from an RC frame structure subject to an earthquake loading testifies to the applicability of the introduced model to the nonlinear dynamic analysis of RC frame structures.

2. Proposed moment-curvature relation

The moment-curvature relation of a section is uniquely defined according to the dimensions of the concrete section and the material properties of concrete and steel. Since the gradient of the moment-curvature relation represents the elastic bending stiffness EI , which includes all the section properties in a typical loading condition, using the moment-curvature relation instead of taking the layered section approach abbreviates the accompanying sophisticated calculations in the non-linear analysis such as the determination of the neutral axis and the change of the elastic stiffness. This is why the non-linear analysis of RC beams based on the moment-curvature relation is used in this study.

Under cyclic loading, the shape of the moment-curvature relation of RC sections is very much governed by the shape of the cyclic stress-strain loop for the steel because the applied moment is carried very largely by the steel reinforcement placed in a section after the first yield excursion. In

addition, the Bauschinger effect of the steel causes the moment-curvature relationships to be curved after the first yield excursion and follows the rounding and pinching in the moment-curvature loops. This implies that there will be less energy dissipation per cycle than in the generally assumed parallelogram of classical elastoplastic behavior (Clough and Johnston 1966, Takeda *et al.* 1970).

All of the hysteretic moment-curvature relations proposed to date are based on the assumption of a perfect bond while defining an initial elastic loading branch. In addition, linear inelastic unloading-reloading branches have been assumed (Clough and Johnston 1966, Chung *et al.* 1998, Roufaiel and Meyer 1987, Spadea and Bencardino 1997). These assumptions, however, may lead to a greater difference in structural response as the deformation increases. Accordingly, to improve the structural behavior of RC beams under cyclic loading and large deformations, the bond slip effect need to be considered, and a curved idealization of the moment-curvature relation, introduced in this paper by referring to the cyclic stress-strain curve of steel (Menegotto and Pinto 1973), takes into account the bond-slip effect. The proposed model is presented in two steps: construction of the monotonic envelope curve and definition of subsequent hysteretic moment-curvature curves; the model can be divided into four different regions as described below.

Region 1 (An initial elastic branch with stiffness EI_{00} in Fig. 1): This region characterizes elastic loading and unloading as long as the positive yield moment M_y or negative yielding moment $-M_y$ is not exceeded. Unlike the previously introduced hysteretic models (Chung *et al.* 1998, Clough and Johnston 1966, Roufaiel and Meyer 1987, Takeda *et al.* 1970), the bond-slip effect is already taken into consideration while defining the initial stiffness EI_{00} in Fig. 1. Selection of an initial elastic branch dominantly affects the structural behavior because it serves as an initial reference asymptote whenever subsequent inelastic unloading or reloading begins (see subsequent asymptotes with EI_{00} in Fig. 1). If it is defined on the basis of the perfect bond assumption as well as the previous models, the stiffness degradation, gradually increased with the increase of deformation, cannot be simulated effectively. If a perfect bond is assumed, the stiffness of the initial unloading asymptote will be greater than EI_{00} , and it will be followed by stiffer subsequent unloading branches than those defined in Fig. 1. Especially at the beam-column joint where the structural response is dominantly

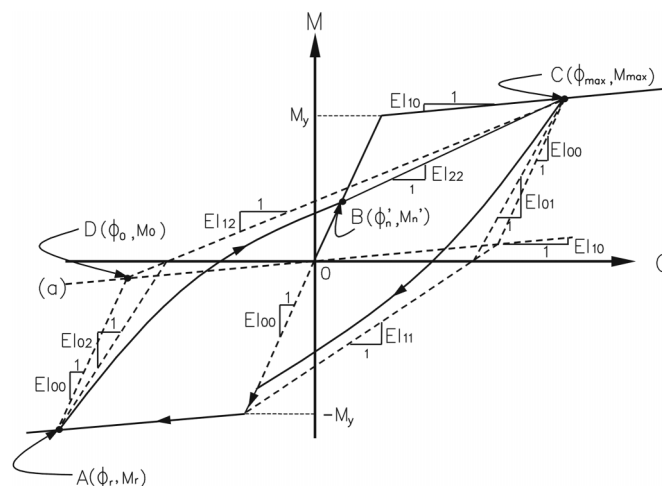


Fig. 1 Proposed moment-curvature relation in beam (Kwak and Kim 2002)

affected by bond-slip, use of the elastic branch considering the bond-slip effect gives a more exact structural response under cyclic loading. More details for the derivation procedure of the monotonic skeleton curve can be found in the previous paper (Kwak and Kim 2002).

Region 2 (curved region of point A to point B in Fig. 1): When unloading or reloading starts, the moment-curvature response of a section initiates with a very similar shape to the stress-strain relation of steel; that trend continues during the closing of cracks because the structural behavior in this region is dominantly affected by the amount of longitudinal tension and compression reinforcement embedded. Consequently, this phenomenon makes it possible to define the moment-curvature relation by the following formula inferred from the hysteretic curve of steel (Pinto and Giuffre' 1970), and its application is limited in the region from the moment reversal point (point A(ϕ_r, M_r) in Fig. 1) to the crack closing moment (point B(ϕ_n', M_n') in Fig. 1) at which the unloading or reloading curve meets the initial elastic branch.

$$M^* = p \cdot \phi^* + \frac{(1-p) \cdot \phi^*}{(1 + \phi^{*G})^{1/G}} \quad (1)$$

$$\text{where } \phi^* = \frac{\phi - \phi_r}{\phi_0 - \phi_r}, \quad M^* = \frac{M - M_r}{M_0 - M_r}$$

Eq. (1) represents a curved transition from a straight line asymptote with slope EI_{0i} to another asymptote with slope EI_{1i} (see Fig. 1) at the i -th load reversal after yielding of the RC section. EI_{0i} is the modified flexural stiffness of the initial elastic stiffness EI_{00} , and the difference between EI_{0i} and EI_{00} represents a progressive stiffness reduction due to concrete cracking and local bond deterioration of the concrete-steel interface. EI_{0i} is somewhat smaller than EI_{00} , and it gradually decreases as deformation increases. The calculation of EI_{0i} can be inferred from Fig. 1. EI_{1i} is the slope of a straight line connecting the point D(ϕ_0, M_0), where the two asymptotes of curve (a) and the initial reference asymptote with slope EI_{00} meet, and the point C(ϕ_{\max}, M_{\max}) where the last curvature reversal with moment of equal sign took place (see Fig. 1). Unlike the steel model where the hardening parameter has a fixed ratio (Menegotto and Pinto 1973, Pinto and Giuffre' 1970), the hardening parameter p in Eq. (1) changes according to the loading history and is assumed to have a ratio between slope EI_{0i} and EI_{1i} at the i -th load reversal because an already cracked section cannot sustain as many moments as an uncracked section due to the presence in the compression region of open cracks. The points D(ϕ_0, M_0) and A(ϕ_r, M_r) will be updated after each curvature reversal.

Two basic changes, compared to the previous straight line approximations, are implemented in this paper: (1) use of the initial elastic branch considering the bond-slip effect; and (2) adoption of the curved hysteretic loop on the range from the moment reversal point to the crack closing moment. The straight lines, which were defined as the unloading and reloading paths in the previous models, are utilized with the asymptotes in defining the curved hysteretic loop in this study.

Moreover, a critical issue in the curved hysteretic loop is the determination of parameter G in Eq. (1), since it influences the shape of the transition curve even though the influence of the G value may not be great in the structural behavior. The G value in Eq. (1), however, cannot be determined easily because the shape of the transition curve depends on many variables, i.e., the amount of compression and tensile steel and its relative ratio, the amount of effective strain hardening, the moment to shear ratio, shape of the cross section, etc. To solve this problem while maintaining the basic concept used in defining ξ , which represents the normalized plastic deformation in the steel model, the layered section approach is adopted on the basis of the material

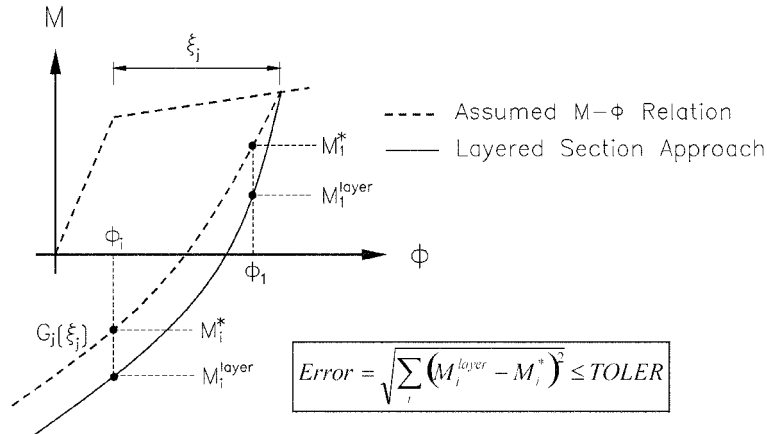
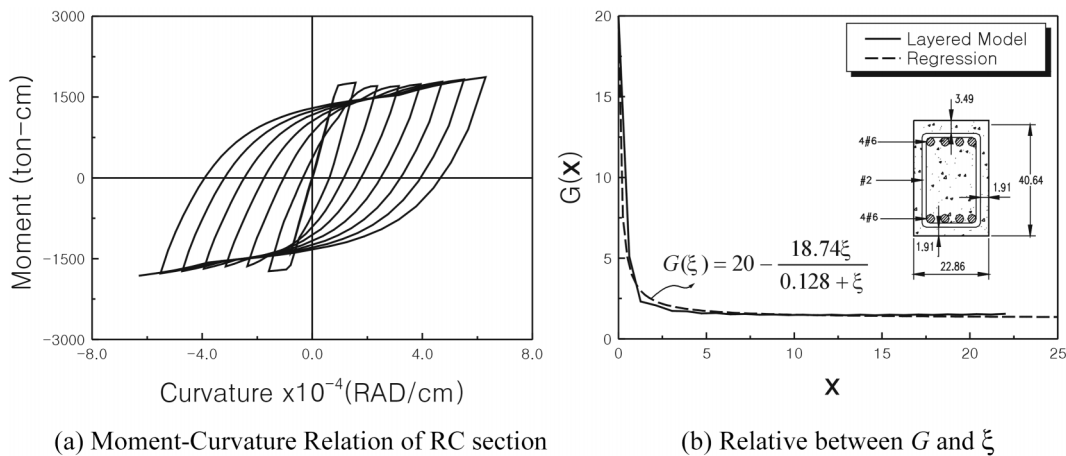


Fig. 2 Calculation of error

models used (Menegotto and Pinto 1973, Taucer *et al.* 1991).

When an RC section is subjected to monotonic or cyclic loading, the moment-curvature relation of the section is uniquely defined according to the dimensions of the concrete section and the material properties of concrete and steel. If the curvature is increased in steps corresponding to the curvature ductility ratio (ϕ/ϕ_y) increments of one unit, the moment-curvature relation can be constructed through the layered section approach, as shown in Fig. 3(a). With an arbitrary assumed G_j value for each ξ_j value, the moment M_i^* corresponding to each curvature ϕ_i can be calculated from Eq. (1). Since the transition curve maintains a convex form due to the dominant influence of steel embedded in a section and since its shape depends on the parameter G_j , the repeated assumptions of G_j by the bi-section method may be continued until the summation of differences between the moment by the layered section approach, M^{layer} , and that by Eq. (1), M^* , satisfies the specified tolerance. In advance, a value G_j corresponding to ξ_j , which gives the minimum difference, can be finally determined on the basis of a square root of the sum of the squares (SRSS). Fig. 2 represents a typical example for the calculation of error norm.



(a) Moment-Curvature Relation of RC section

(b) Relative between G and ξ

Fig. 3 Determination of G value

After determining the values G_j that correspond to each ξ_j , the relation between G and ξ is constructed by the nonlinear regression. Fig. 3 shows the analytically constructed moment-curvature relation, the variation of G according to the loading history for a typical section, and the obtained regression curve of $G(\xi)$. The same G_0 value used in the steel model is assumed.

During unloading and reloading from an inelastic, a significant reduction in stiffness occurs as the number of alternating loading cycles increases. Accordingly, neglecting loss of stiffness may lead to an over-estimation of the energy absorption capacity of the structure and also to a reduction of load carrying capacity of the structure. Most importantly, the constitutive model for the hysteretic moment-curvature curve proposed to date considers the stiffness degradation on the basis of the Takeda model (1970). The same rule is also taken into consideration in this paper (see Fig. 1).

Region 3 (linear region from point B to point C in Fig. 1): The second branch of the reloading curve describes the behavior after crack closure up to the second branch of the primary moment-curvature curve. Since the structural behavior in this region represents the proportional increment of the load carrying capacity, the moment-curvature curve is assumed with the following linear relation

$$M = EI_{2i} \cdot \phi + (M_{\max} - EI_{2i} \cdot \phi_{\max}) \quad (2)$$

where EI_{2i} is the slope of straight-line connecting the points B(ϕ'_n, M'_n) and C(ϕ_{\max}, M_{\max}) at the i -th load reversal.

Region 4 (yielding region after the point C in Fig. 1): The second branch of the primary moment-curvature curve can be expressed as:

$$M = EI_{10} \cdot \phi + (M_{\max} - EI_{10} \cdot \phi_{\max}) \quad (3)$$

where EI_{10} is flexural stiffness of the monotonic envelope after yielding.

3. Modification of moment-curvature relation

3.1 Shear effect on moment-curvature relation

As is well known through experimental study (Fang *et al.* 1993, Ma *et al.* 1976, Popov *et al.* 1972), for beams with a shorter span or with a higher nominal shearing stress, it takes fewer cycles to reach failure and the recorded load-deflection hysteretic loops exhibit a progressive pinching of loops due to shear deformations. This in turn leads to a reduction in the energy dissipation capacity of the beam. To reflect the pinching effect according to the shear span length into a hysteretic moment-curvature relation representing the bending behavior, Meyer *et al.* (1987) proposed a modification of the reloading branch on the basis of the empirical results (Ma *et al.* 1976, Popov *et al.* 1972). Because of its simplicity in application and computational convenience, determination of the characteristic point B'(ϕ_p, M_p) on the original elastic loading curve, by which the new asymptote with the bending stiffness EI_{1i}^p is defined (see Fig. 4), follows the same criteria as those proposed by Meyer *et al.*

$$M_p = \alpha_p \cdot M_n, \quad \phi_p = \alpha_p \cdot \phi_n \quad (4)$$

where $\alpha_p = 0$ for $a/d < 1.5$, $\alpha_p = 0.4 \cdot a/d - 0.6$ for $1.5 < a/d < 4.0$, $\alpha_p = 1$ for $a/d \geq 4.0$, a = the shear span length, d = the effective depth of a section, and M_n and ϕ_n are the moment and curvature at the point N(ϕ_n, M_n) in Fig. 4.

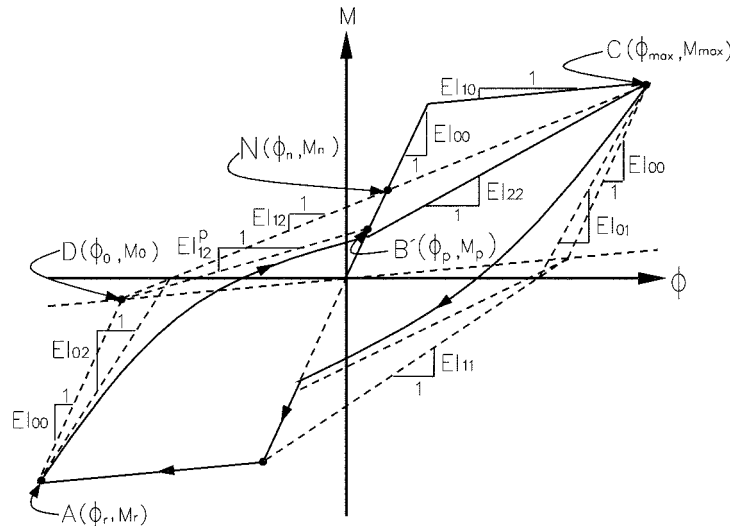


Fig. 4 Consideration of shear effect

Namely, the pinching effect is taken into consideration in the hysteretic moment-curvature relation by using EI_{1i}^p , the slope of asymptote connecting points $D(\phi_0, M_0)$ and $B'(\phi_p, M_p)$, instead of EI_{1i} used in Fig. 1. The hardening parameter p of the curved reloading branch is determined on the basis of the two straight line asymptotes with stiffness EI_{0i} and EI_{1i}^p (see Fig. 4).

3.2 Axial force effect on moment-curvature relation

When an RC beam section is subjected to axial load, no unique moment-curvature relation can be expected because the axial load influences the curvature. As inferred from the $P - M$ diagram of an RC section, the ultimate resisting moment M increases almost proportionally to the axial load P until the RC section reaches the balanced failure point in the $P - M$ intersection diagram. However, it is evident that the ductility of the section is significantly reduced by the presence of the axial load. Because of the brittle behavior of an RC section at even moderate levels of axial compressive load, to improve the ductility of the RC section, the ACI 318 (1995) recommends that the ends of columns in ductile frames in earthquake areas must be confined by closely spaced transverse reinforcement when the axial force is greater than 0.4 of the balanced load P_b .

In advance, as well known through the experimental studies (Low and Moehle 1987, Park *et al.* 1972, Wight and Sozen 1975), the hysteretic moment-curvature relation of an RC section subjected to axial load represents a marked pinching of loops because the axial force acts to close open cracks and cause a sudden increase in stiffness after crack closing. Consequently, ignoring the increase of the ultimate resisting moment and the pinching phenomenon in the RC beams subjected to the axial force may lead to an incorrect structural response. However, as mentioned in previous experimental studies (Low and Moehle 1987, Park *et al.* 1972, Wight and Sozen 1975), the presence of an axial compressive load slows the decay in strength and stiffness of RC beams with cycling and relieves the pinching phenomenon by the shear force. Therefore, it may not be necessary to consider the axial force effect simultaneously with the shear force effect while defining a hysteretic moment-curvature relation.

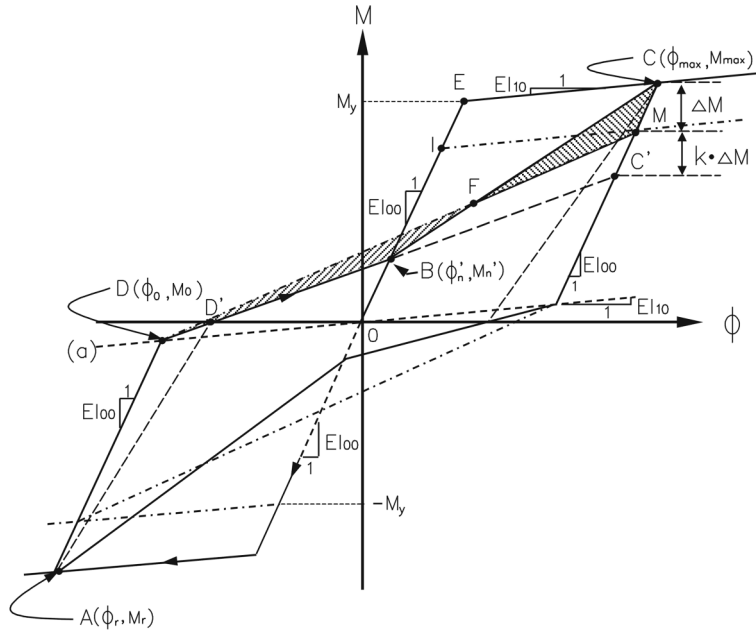


Fig. 5 Consideration of axial force effect

To reflect the axial force effect into a hysteretic moment-curvature relation, modifications of the monotonic skeleton curve and of the unloading and reloading branches are required. Firstly, the monotonic skeleton moment-curvature curve (\overline{OEC} in Fig. 5) can be constructed by beam analysis with an axial force in accordance with the proposed algorithm in the companion paper. If it is assumed that the line \overline{OIM} in Fig. 5 corresponds to the monotonic skeleton curve for the beam without an axial force in Fig. 1 and the line \overline{DFM} in Fig. 5 to the straight line asymptote \overline{DC} in Fig. 1, respectively, then the modified asymptote \overline{DBC} in Fig. 5 can be constructed on the basis of the energy equilibrium condition.

Since external work by axial force lower than the balanced load P_b can be ignored due to the negligibly small axial deformation, the internal energy represented by the area within the hysteretic loop must maintain a constant value regardless of the applied force. This implies that the area of the triangle ΔDBF will be the same as that of the triangle ΔFMC in Fig. 5. Point B in Fig. 5 which defines the modified crack closing point, is finally determined through calculation of the constant k in Fig. 5. When the constant k is represented by $k = (M_m - M_c) / (M_{max} - M_m)$, it can be simplified as the following equation from the area equality of two triangles ($\Delta DBF = \Delta FMC$):

$$k = \frac{M_y - M_{max}}{M_0} \tag{5}$$

Moreover, the remaining procedures to define the curved reloading and unloading branches and the following straight line branches are the same as those introduced in the proposed moment-curvature relation in Fig. 1. Finally proposed moment-curvature relation considering axial force effect can be seen in Fig. 6.

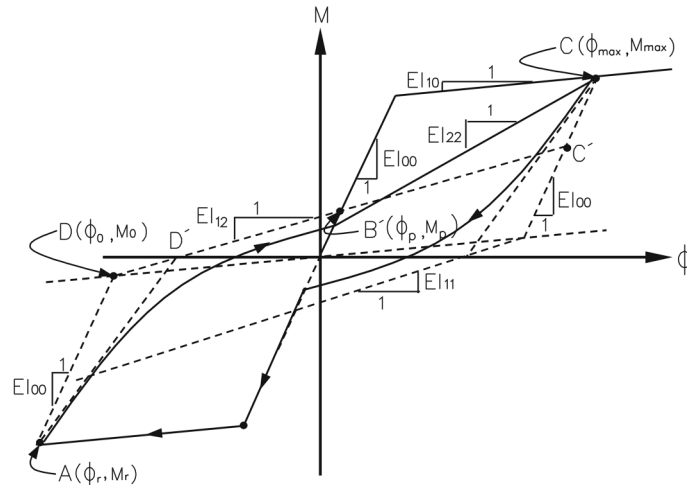


Fig. 6 Proposed moment-curvature relation considering axial force effect

3.3 Consideration of fixed-end rotation

Unlike the critical region located in the vicinity of beam mid-span as well as the ends of long-span beams, the behavior of the critical region at the beam-column joint of relatively short-span beams may be greatly affected both by the shear and also by the details of anchoring the beam reinforcements. In particular, slippage of the main bars from the anchorage zone accompanies the rotation of the beam fixed-end, θ_{fe} , which cannot be simulated with any mechanical model, and this rigid body deformation may be increased as the deformation increases (see Fig. 7). Consequently, its exclusion may lead to an over-estimation of the energy absorption capacity of the structure. Accordingly, to simulate the structural behavior more exactly, we need to take into account the fixed-end rotation because most of the structural behaviors under lateral loads are concentrated at the beam-column joints with narrow width, especially in the case of slender multi-story buildings.

This range is called the plastic hinge length. Various empirical expressions have been proposed by investigators for the equivalent length of the plastic hinge length l_p . Since the structure is modeled with beam elements whose displacement field is defined by the average deformation of both end nodes, the ultimate capacity can be overestimated if the plastic hinge length is not precisely taken into consideration. In this study, the relatively simple equation of $l_p = 0.25d + 0.075z$, proposed by Sawyer (1964), was used, where d and z are the effective depth of section and distance from the critical section to the point of contraflexure, respectively. Since the plastic hinge length increases in proportion to the axial force, therefore, it may be difficult to estimate the plastic hinge length of an axially loaded member by this simple equation only. Accordingly, the plastic hinge length of $l_p = xh$ proposed by Bayrak and Sheikh (1997) was established as an upper limit value for the plastic hinge length, where h is the section depth and x is the experimental parameter ranged from 0.9 to 1.0.

To account for the fixed-end rotation in the numerical analyses, it is common to reduce the stiffness, EI , in the moment-curvature relation for the elements located at the ends of beam with the range of the plastic hinge length l_p (see Fig. 8(b) and Fig. 9). If a beam with the rotational stiffness k_θ at both ends is subjected to a horizontal force P , as shown in Fig. 8(a), the corresponding horizontal drift Δ_1 can be obtained.

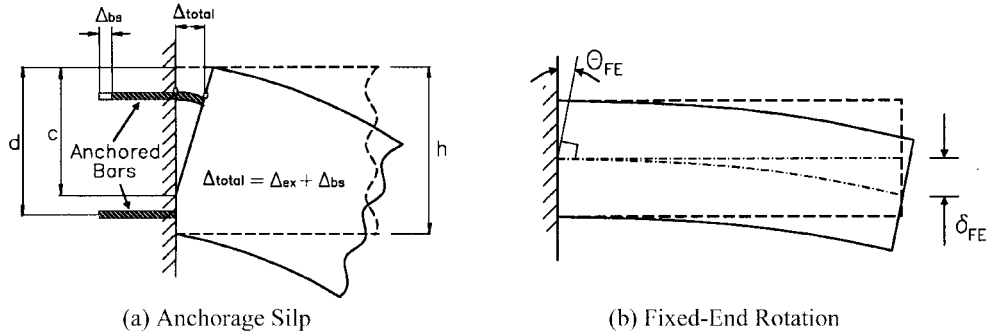


Fig. 7 Rigid body deformation at the beam-column joint

$$\Delta_1 = \frac{PL^3}{12EI} + \frac{PL^2}{2k_\theta} \tag{6}$$

where the first term means the contribution by the bending deformation of the beam and the second term by the end rotational stiffness k_θ .

When the same force acts on a beam with the reduced stiffness EI_{eq} at the both ends, as shown in Fig. 8(b), the horizontal deflection Δ_2 also can be calculated by the moment area method.

$$\Delta_2 = \frac{P(EI_{eq}L_2^3 + 2EIL_p(4L_p^2 + 6L_pL_2 + 3L_2^2))}{12EI_{eq}EI} \tag{7}$$

From the equality condition of $\Delta_1 \equiv \Delta_2$, the equivalent stiffness EI_{eq} can be determined by

$$\frac{1}{EI_{eq}} = \frac{1}{\beta \cdot k_\theta \cdot L} + \frac{1}{EI} \tag{8}$$

Where $\beta = \alpha(1 - 2\alpha + 4/3\alpha^2)$, $\alpha = l_p/L$

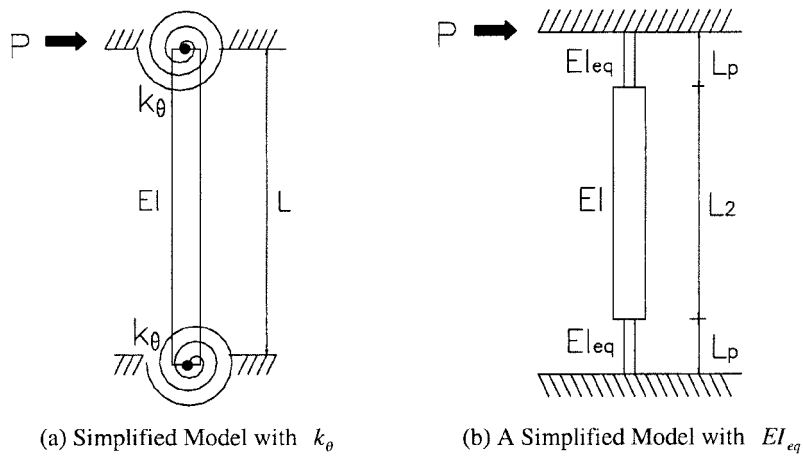


Fig. 8 Consideration of the equivalent stiffness

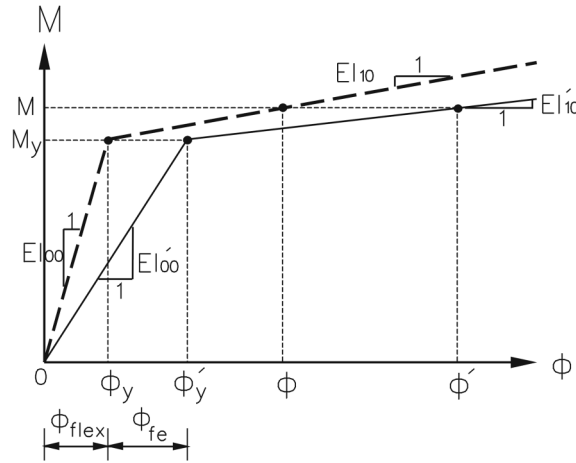


Fig. 9 Modification of monotonic envelope curve

The same derivation procedure for the cantilevered beam is applied and the equivalent stiffness EI_{eq} obtained in this case has the same form as Eq. (8) except the parameter β has the form of $\beta = \alpha(1 - \alpha + 1/3\alpha^2)$

From the above equation, if the stiffness ratio α_{fe} is defined by $\alpha_{fe} = EI/EI_{eq}$ the modified curvature can be expressed as $\phi' = \alpha_{fe}\phi_{flex}$ where ϕ_{flex} represent the curvature at the fixed-end of the beam due to the flexural behavior. The modified stiffness of the initial elastic branch, EI'_{00} , and that of the following inelastic branch, EI'_{10} , can be defined by $EI'_{10} = EI_{10}/\alpha_{fe}$ from the relations of $M_y = EI_{00}\phi_y = EI_{eq}\phi'_y = EI_{eq}\alpha_{fe}\phi_y$ and $M - M_y = EI_{10}(\phi - \phi_y) = EI'_{10}(\phi' - \phi'_y)$ where ϕ_y and M_y are the curvature and moment at the yielding of a section, respectively (see Fig. 9).

However it is almost impossible to conduct experiments on all the beam elements used in a structure to obtain the rigid body rotation or deflection of each member. In this case, the relation between the steel stress and crack width, introduced on the basis of analytical or experimental studies, can be utilized (Harajli and Mukaddam 1988, Monti *et al.* 1997, Oh 1992, Saatcioglu *et al.* 1992). By assuming that a half of the crack width, when the steel yields at the laterally loaded RC beams, corresponds to the anchorage slip of the reinforcing bar, Δ_{fe} , the rotational stiffness k_θ can be defined by

$$\theta_{fe} = \frac{\Delta_{fe}}{d - c}, \quad k_\theta = \frac{M_y}{\theta_{fe}} \tag{9}$$

where c is the distance from the extreme compression fiber to the neutral axis. The neutral axis depth c maintains an almost constant value of $c = \alpha \cdot d$ from the initial cracking up to the yielding of the reinforcing steel.

4. Solution algorithm

For the analysis of RC beams, Timoshenko beam theory was used in this study (Owen and Hinton 1980). Since this theory is well established and widely used in the analysis of beams, more details for the formulation of beam elements can be found elsewhere (Owen and Hinton 1980). In a typical

Timoshenko beam, it is usual to assume that normal to the neutral axis before deformation remains straight but not necessarily normal to the neutral axis after deformation. In addition, the effects of shear deformation are not taken into consideration in simulating nonlinear behavior since the normal bending stresses reach a maximum at the extreme fibers, where the transverse shear stresses are at their lowest value, and reach a minimum at mid-depth of the beam, where the transverse shear stresses are highest. Thus, the interaction between transverse shear stresses and normal bending stresses is relatively small and can be ignored. This means that the flexural rigidity EI is replaced by that corresponding to the curvature calculated from the nodal displacements by $\phi = (\theta_i - \theta_j)/l$, whereas the shear rigidity of beam element GA is assumed to be unchanged, where θ_i and θ_j mean the rotational deformations at the both end nodes, and l is the element length.

Since the global stiffness matrix of the structure depends on the displacement increments, the solution of equilibrium equations is typically accomplished with an iterative method through the convergence check. The nonlinear solution scheme selected in this study uses the tangent stiffness matrix at the beginning of each load step in combination with a constant stiffness matrix during the subsequent correction phase; that is, the incremental-iterative method. All the remaining algorithms from the construction of an element stiffness matrix to the iteration at each load step are the same as those used in the classical nonlinear analysis of RC structures. More details can be found elsewhere (Kwak and Filippou 1990, Kwak and Kim, S.P. 2001, Kwak and Kim, D.Y. 2001, Owen and Hinton 1980).

In this paper, only the dynamic equilibrium equation for a multi-degrees of freedom system is briefly introduced. When a structure is subjected to ground acceleration \ddot{u}_g , the incremental equation of dynamic equilibrium can be written as

$$M\Delta\ddot{u} + C\Delta\dot{u} + K\Delta u = \Delta P = -M\{1\}\Delta\ddot{u}_g \quad (10)$$

where Δu , $\Delta\dot{u}$ and $\Delta\ddot{u}$ are the incremental displacement, velocity, and acceleration vectors during the time step Δt , respectively. M , C , and K are the mass, damping, and stiffness matrices, respectively. ΔP is the increment of external loads during the time step Δt and is given by $\Delta P = -M\{1\}\Delta\ddot{u}_g$, where $\{1\}$ is a unit vector. A lumped mass matrix M and Reyleigh damping matrix C are used in the analysis. The time history analysis of a structure is based on the average acceleration method which is one of two special cases of Newmark's method because it does not require iteration in solving Eq. (10). More details can be found in the reference (Chopra 1995).

5. Numerical applications

5.1 RC beams subject to cyclic loadings

In order to establish the applicability of the proposed hysteretic moment-curvature relation, two RC beams are investigated and discussed. These beams are specimen 40.048 (COLUMN1) experimented on by Wight and Sozen (1975) and specimen 1 (COLUMN2) experimented on by Low and Moehle (1987). The material properties of each specimen are summarized in Table 1.

The first specimen 40.048 consists of a reinforced concrete cantilever beam with a span length of 87.6 cm, which was subjected to cyclic concentrated lateral and axial loads at the free end (see Fig. 10). The plastic deformation is concentrated at the end of the beam with narrow width,

Table 1 Material properties used in application

SPECIMEN	E_c (kg/cm ²)	E_s (kg/cm ²)	f_c (kg/cm ²)	f_y (kg/cm ²)	ρ (A_{st}/bd)	ρ' (A_{sc}/bd)	P (kg)
COLUMN1	244643	2046625	266	5060	0.012	0.012	18160
COLUMN2	310684	2046625	429	5060	0.010	0.010	4545

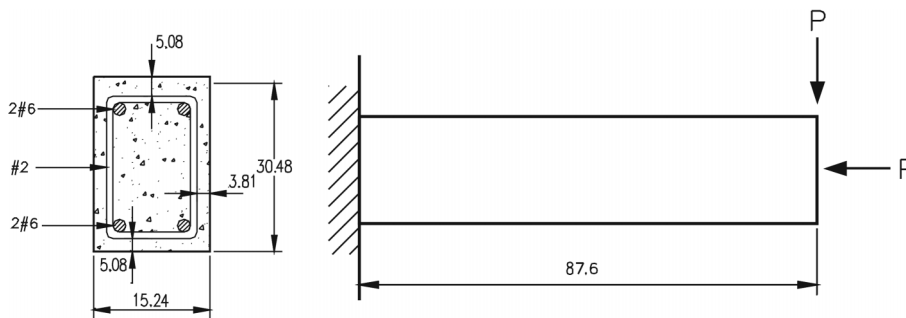


Fig. 10 Details of COLUMN1 (unit: cm)

accompanying fixed-end rotation that occurs in addition to elastic rotation at the large deformation stage. To simulate more exact structural behavior with the beam element formulated on the basis of the average deformation in an element, separate consideration of this region is required in the finite element modeling. The plastic hinge length, l_p , is determined to be 20 cm, which is three times greater than the concrete cover. Accordingly, the specimen is modeled along the entire span with an element of $l = 10$ cm.

As introduced by the load-deflection relations shown in Fig. 11, a direct application of the Takeda model (1970), which was designed for a beam element without an axial load, leads to an incorrect

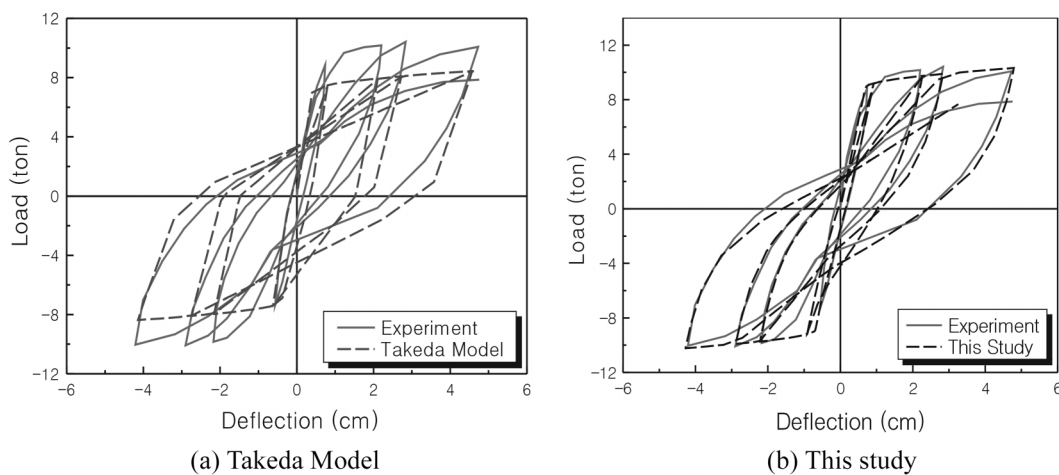


Fig. 11 Load-deflection relation of COLUMN1

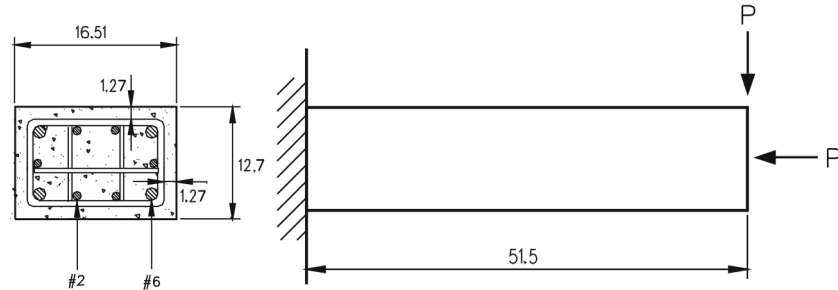


Fig. 12 Details of COLUMN2 (unit: cm)

structural response. This is because the classical hysteretic moment-curvature relations for the beam element (Clough and Johnston 1966, Dowell *et al.* 1998, Roufaiel and Meyer 1987, Takeda *et al.* 1970) do not take into account the increase of the ultimate resisting moment and the pinching phenomenon due to the axial load. On the other hand, the proposed model effectively estimates the ultimate resisting capacity and simulates the pinching phenomenon even at the large deformation stage (see Fig. 11(b)). Accordingly, more exact prediction of structural response for RC columns and/or prestressed concrete beams subjected to an axial force requires the consideration of the axial force effect.

The second specimen (COLUMN2) is selected to show the effects of bond-slip and fixed-end rotation on the structural response. The geometry and cross section dimensions are presented in Fig. 12, and this example structure is modeled along the entire span with an element of $l = 5$ cm from consideration of the plastic hinge length.

This structure was analyzed by Filippou *et al.* (1991) on the basis of the layered section approach, and Fig. 13(a) shows the obtained load-deflection relation. Unlike the Takeda model (1970), the numerical results by Filippou *et al.* also simulate the ultimate resisting capacity effectively because the axial force effect is included in their formulation by considering the axial force equilibrium condition on a section. However, the layered section approach represents slightly stiffer structural behavior than the experimental data. This difference seems to be caused by ignoring the bond-slip effect and fixed-end rotation. Since the layered section approach is based on equilibrium and compatibility conditions between each imaginary layer, the bond-slip effect cannot be taken account, and unrealistic stiffer structural behavior deepens as the deformation increases, following overestimation of the energy absorbing capacity of a structure. In particular, the stiffness degradation is generally accompanied by a decrease of shear stiffness as the deformations increase. However, the layered section approach has a limitation in simulating this phenomenon because it is based on the bending behavior.

On the other hand, as shown in Fig. 13(b), the proposed model effectively simulates the stiffness degradation and pinching phenomenon due to the application of axial load. This result seems to arise from the fact that the bond-slip effect and fixed-end rotation have already been included during construction of the monotonic skeleton curve of the moment-curvature relation (see Fig. 1). More comparison of analytical results with experimental studies for RC beam members can be found elsewhere (Kwak and Kim 1998, 2002).

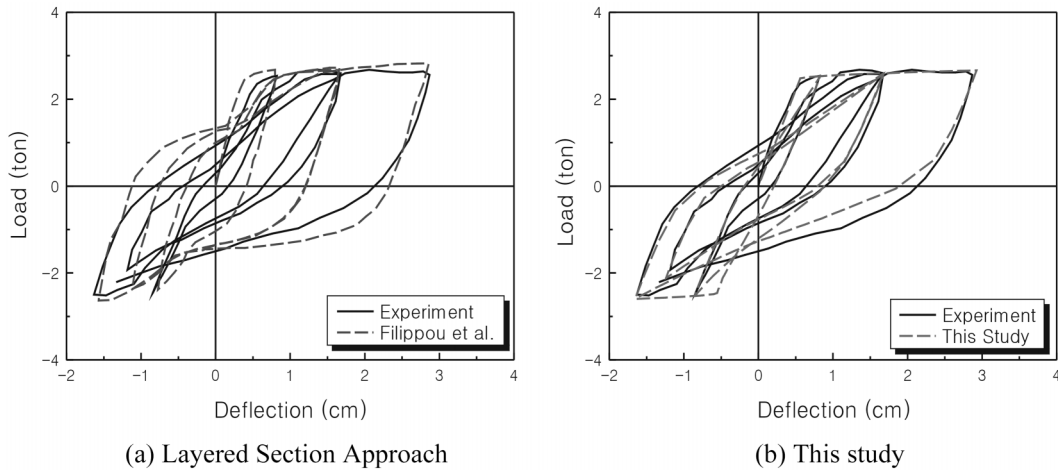


Fig. 13 Load-deflection relation of COLUMN2

5.2 RC frame structure subject to dynamic loading

The ability of the introduced model in describing the dynamic response of RC frame structures is assessed by correlation study between analytical and experimental results. The RC frame structure is specimen RCF2, which has been tested on the shaking table by Clough and Gidwani (1976). As shown in Fig. 14, this structure is a two-story, one-bay RC frame subject to a simulated strong base motion and is a 0.7 scale model of a two-story office building representative of common design and construction practice. The concrete blocks were added on every floor to take into account the influence by the floor mass and self-weight when a base acceleration acts, and the N69W Taft record from the Arvin-Tahachapi earthquake of July 1952, scaled to peak acceleration of 0.57 g and referred to as W2 (see Fig. 15), was used.

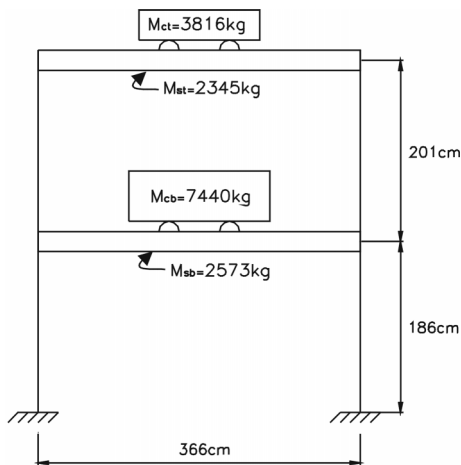


Fig. 14 Idealization of RCF2

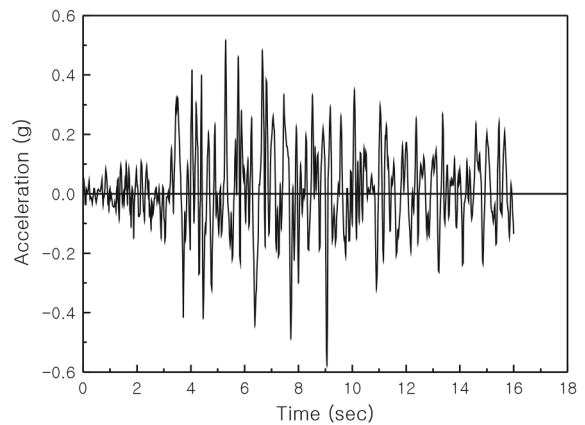


Fig. 15 N69W Taft Record W2, Scaled to 0.57 g

Table 2 Section properties used in RCF2

Member	Story	M_y^+ ($10^3 \text{ kg} \cdot \text{cm}$)	EI^+ ($10^6 \text{ kg} \cdot \text{cm}^2$)	M_y^- ($10^3 \text{ kg} \cdot \text{cm}$)	EI^- ($10^6 \text{ kg} \cdot \text{cm}^2$)
Girder	Bottom	267	4480	829	4480
	Top	236	3476	737	3477
Column	Bottom	239	1141	239	1141
	Top	223	1463	223	1463

Since the response of this frame structure is dominantly affected by flexural and anchorage slip of reinforcing bar but strength degradation due to shear deformations is expected to be small, the influence of the anchorage slip on the nonlinear response of RC frame structure can effectively be investigated through this example structure. The nonlinear responses of RC columns seem to be more remarkable in this example structure than with most building structures because smaller bending stiffness EI are assigned to columns (see Table 2). The geometry and reinforcing details of the test frame as well as the arrangement of the shaking table and the conduct of the test are described in detail in Reference (Clough and Gidwani 1976). Also, the section properties mentioned by Dámbrisi and Filippou (1997) are used for the correlation study in this paper. The values of section properties for each member can be found in Table 2. The axial force effect is taken into consideration in these values. According to the equation proposed by Saywer (1964), the plastic hinge length l_p is determined to be 20 cm. Therefore, the end regions of each member are modeled with an element of $l = 5 \text{ cm}$, and the other regions at each member are equally idealized by using 10 elements.

The time history response of the example structure, obtained by using the Takeda model in which the linear inelastic unloading-reloading branches have been assumed, are compared with experimental data in Fig. 16 and Fig. 17 because this linear model is popularly used in the time history analyses (Takeda *et al.* 1970). First, as shown in Fig. 16 representing the time histories for the bottom and top floor displacement, a little difference between experimental and analytical results is observed. In particular, in spite of the quite satisfactory agreement in the maximum displacement values, a slight phase shift at the initial stage results in a noticeable discrepancy between the experimental and analytical results in the last stage of the response time history. This phenomenon seems to be caused by the overestimation of the structural stiffness. Because the bond-slip effect is not taken into account in the Takeda model, the bending stiffness EI at the unloading, reloading, and loading phases is overestimated, and this accompanies the underestimation of deformations and a decrease in the response period in the analytical results as the time history continues.

In advance, as mentioned in the previous example structure COLUMN1, a direct application of the Takeda model leads to an incorrect structural response because the axial force effect is not considered. Correlations of story shear between analytical results by Takeda model in Fig. 17 and experimental data in Fig. 18 also show that the Takeda model slightly underestimates the ultimate resisting capacity of columns located at bottom and top story and pinching phenomenon is not effectively simulated. This result indirectly explains why the classical hysteretic moment-curvature relations designed for the beam element can not be used without any modification in the analysis of a beam subjected to a relatively large axial load.

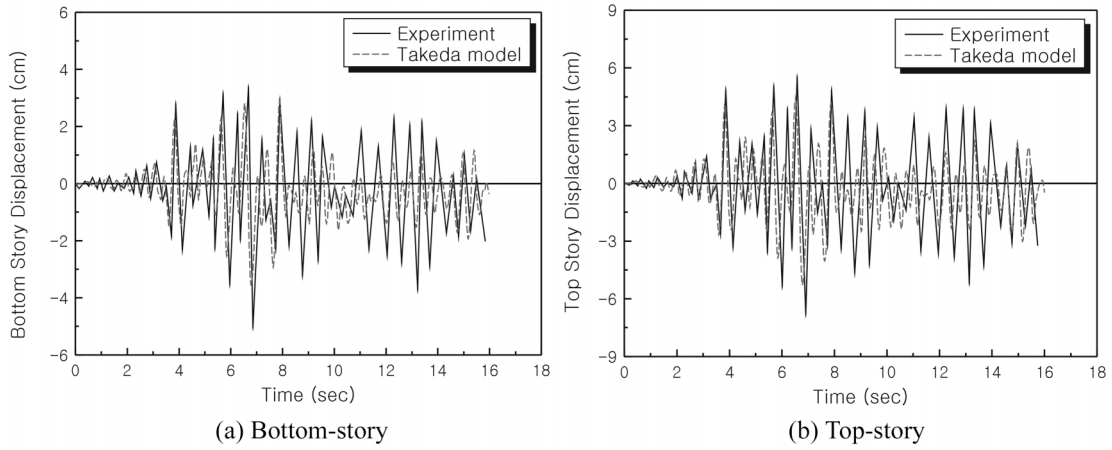


Fig. 16 Correlation of displacement response using Takeda model

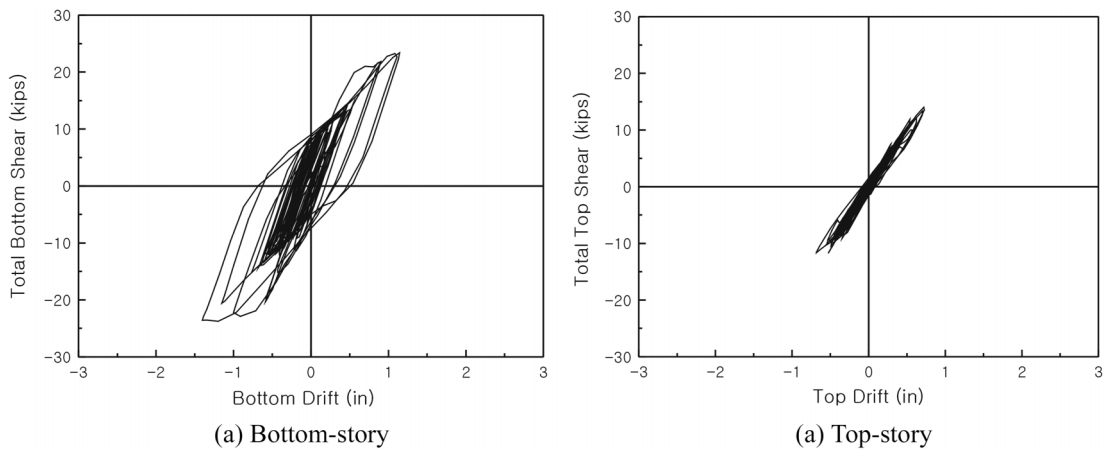


Fig. 17 Relation between story shear and story drift by Takeda model

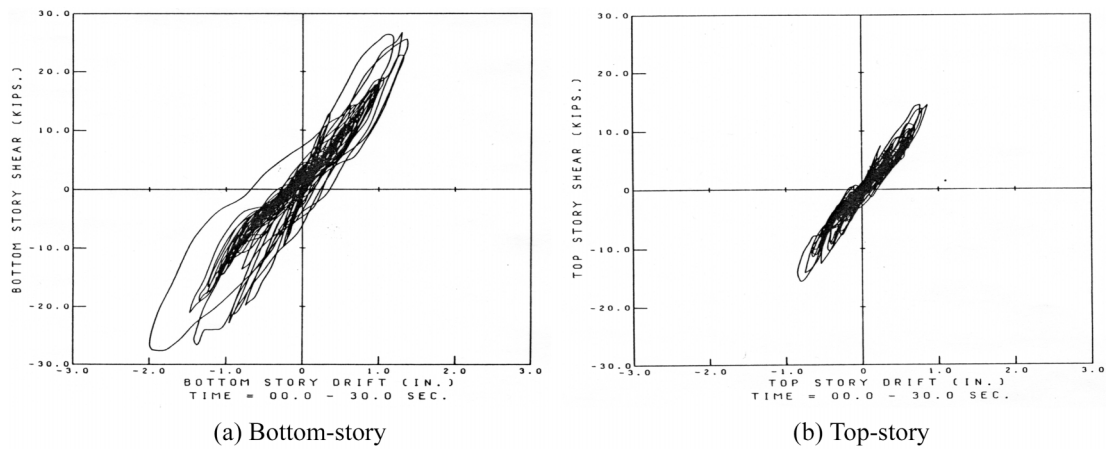


Fig. 18 Relation between story shear and story drift by experiment

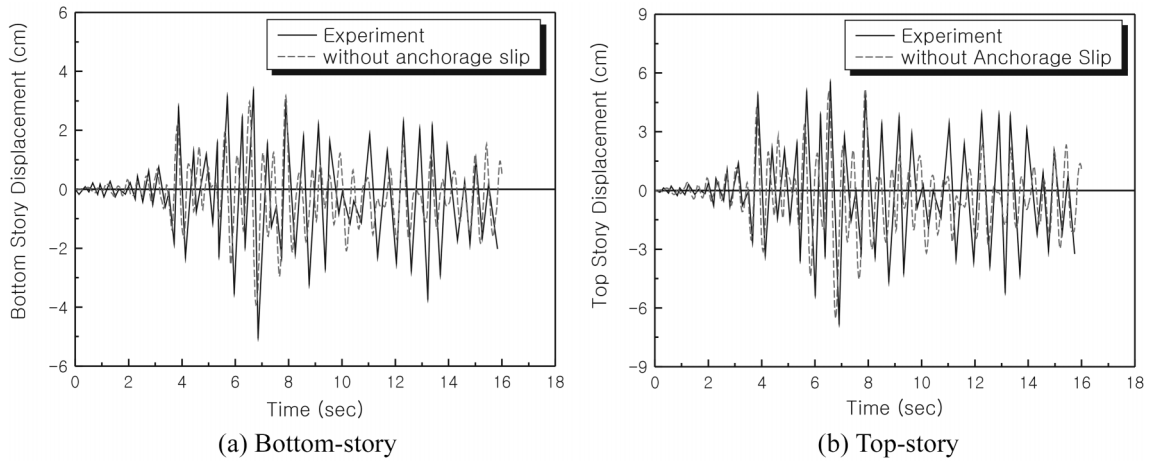


Fig. 19 Correlation of displacement response ignoring the anchorage slip effect

The numerical results obtained on the basis of a hysteretic moment-curvature relation with the monotonic skeleton curve constructed by considering the axial force effect (see Fig. 5) are shown in Fig. 19. Still, a noticeable discrepancy between experimental and analytical results remains in this figure in spite of consideration of the axial force effect. This difference can be attributed to an inaccurate consideration or exclusion of the anchorage slip concentrically occurred at the end region of each member. Fig. 19 also shows that the overestimation of the stiffness induced by ignoring the anchorage slip causes a slight phase shift at the initial loading stage results but leads to a remarkable decrease in the structural displacement as the loading stage continues while representing an increasing discrepancy between the experimental and analytical results. Therefore, the quite satisfactory correlation between experiment and analysis can not be expected without considering the anchorage slip effect.

As mentioned in Eq. (8), determination of the equivalent stiffness EI_{eq} with consideration of the anchorage slip effect requires the calculation of the end rotational stiffness k_{θ} . Therefore, the value $k_{\theta} = 57.6 \times 10^6 \text{ kg} \cdot \text{cm}$ as determined by Dámbrisb and Fillippou (1997) on the basis of the numerical simulation is also adopted in this paper. As mentioned before, however, the end rotational stiffness k_{θ} can not be usually defined as a unique value prior to the numerical simulation, and it is also impossible to conduct experiments for all the members in a structure to obtain the rigid body rotation. In this case, the analytical approach introduced in Eq. (9) can be used. The plastic hinge length and the equivalent stiffness mentioned in Eq. (8) are $l_p = 20 \text{ cm}$ and $EI_{eq} = 639 \times 10^6 \text{ kg} \cdot \text{cm}^2$, respectively, in this example structure.

Fig. 20 and Fig. 21 show the final numerical results, which represent very good agreement with experimental results. Comparison of these figures with Fig. 19 and Fig. 17 indirectly illustrates why the previous numerical models may have some difficulties in the modeling of beam-column joints and why the fixed-end rotation and the pinching effect due to the applied axial must be taken into consideration to obtain a more realistic simulation of the structural behavior. If the anchorage-slip effect is not considered, larger differences from the experimental data are expected in the dynamic loading case than in the cyclic loading and/or monotonic loading cases since the slopes of the initial elastic branch and subsequent inelastic unloading-reloading curves in a hysteretic moment-curvature

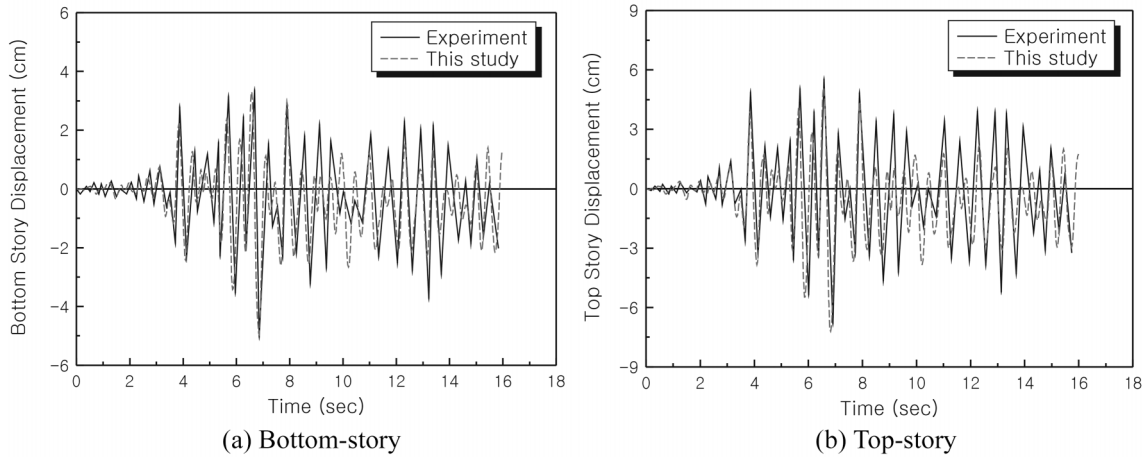


Fig. 20 Correlation of displacement response considering the anchorage slip effect

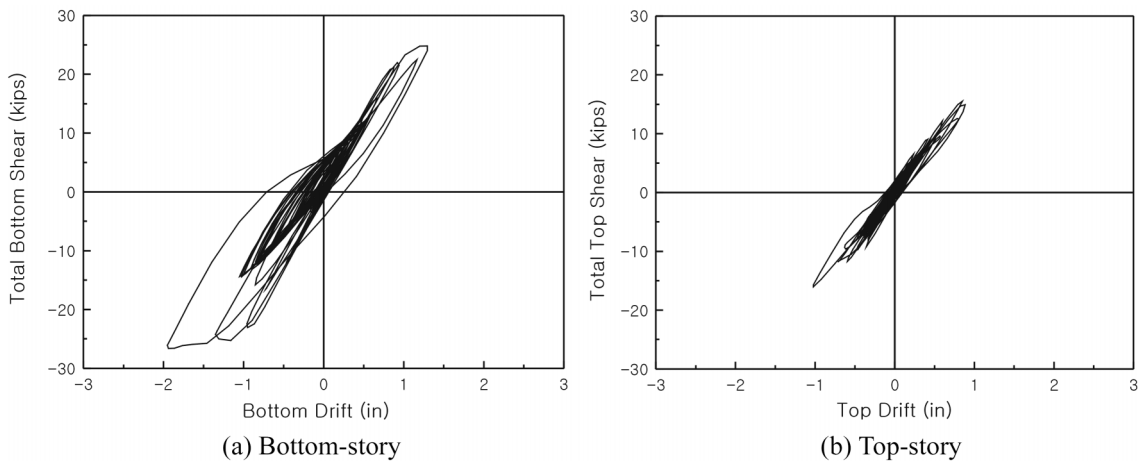


Fig. 21 Relation between story shear and story drift by the introduced model

relation are overestimated. This overestimation may cause a rapid decrease in the structural response as the loading stage increases and also may give a different collapse condition from the experiment when a structure with multi-degrees of freedom is subjected to a severe dynamic loading.

Careful investigation of the obtained numerical results in Fig. 20 and Fig. 21 yields the following observations: (1) The maximum response value for the bottom story displacement is increased by more than 30% as the anchorage slip effect is taken into account; (2) In general, very satisfactory agreement between experimental and analytical results is observed for the displacement time histories through the entire time range. Nevertheless, a slight discrepancy still exists in the last stage of the response time history. This result seems to be caused by the fact that a gradual stiffness degradation, even at the same loading condition, is induced in the experiment after the yielding of reinforcing bar due to an increase of crack opening and anchorage slip; (3) The story shears in Fig. 21 reveal that most nonlinear responses and damages to the example structure are concentrated

at the bottom-story columns, while the top-story columns suffer little damage. The characteristic pinching of the hysteretic relation, caused by the axial force effect and the anchorage slip, seems to be evident in Fig. 21(a). Moreover, this figure indirectly explains the importance of considering the plastic hinge region in a member, where decrease of the bending stiffness are concentrated; (4) Finally, these figures confirm that the numerical model introduced in this paper can effectively be applied to the nonlinear dynamic analysis of RC frame structures.

6. Conclusions

This paper concentrates on the introduction of a moment-curvature relation of an RC section that can simulate the cyclic behavior of RC beams. Unlike most mathematical or mechanical models found in the literature, the proposed model has taken into account the bond-slip effect, the Bauschinger effect of the steel, axial force effect, and fixed-end rotation at the fixed end of a beam. A modification of the proposed moment-curvature relation has also been introduced to take into account the stiffness degradation and pinching effect on the basis of the Meyer model (1987) in the case of shear dominant structures. A modification of the hysteretic moment curvature relation to consider an increase of the ultimate resisting capacity and the pinching phenomenon in the axially loaded RC beams is also introduced on the basis of the energy conservation. The application of the proposed model extends to an RC frame structure subject to dynamic loading. However, in spite of many numerical and mechanical models considering the strength degradation (Chung *et al.* 1998, Dowell *et al.* 1998, Takeda *et al.* 1970) and axial hysteretic behavior (Cheng 2001), these effect are not included in the proposed model. An additional concern for the strength degradation under cyclic loading beyond the yield strength may be required to estimate the exact damage level undergone by a section after a certain number of cycles. The system identification (SI) method may be applied to construct a strength degradation model that can give a more rational damage assessment. Furthermore, since vertical ground motion can cause columns in tension and compression, relation between axial and transverse hysteretic behavior can be considered in order to achieve a comprehensive response behavior.

Through correlation studies between analytical results and experimental values from typical RC beam and frame tests, the following conclusions are obtained: (1) The inclusion of pinching effect is important in structures dominantly affected by shear; (2) to accurately predict the structural behavior of the beam to column subassembly where the nonlinear response is concentrated, a modification of the moment-curvature relation to consider the fixed end rotation due to anchorage slip is strongly required; (3) to effectively simulate axially loaded RC beams, the axial load effect must be considered; and, finally, (4) the proposed model can be effectively used to predict the structural response under cyclic loading, and its application can effectively be extended to the dynamic analysis of a frame structure.

Acknowledgements

The research presented in this paper was sponsored by the Smart Infra-Structure Technology Center. Their support is greatly appreciated.

References

- ACI 318 (1995), *Building Code Requirements for Structural Concrete*.
- Assa, B. and Nishiyama, M. (1998), "Prediction of load-displacement curve of high-strength concrete columns under simulated seismic loading", *ACI Structural Journal*, **95**(5), 547-557.
- Bayrak, O. and Sheikh, S.A. (1997), "High-strength concrete columns under simulated earthquake loading", *ACI Structural Journal*, **94**(6), 708-722.
- Cheng, F.Y. (2001) "Cheng-Lou axial hysteresis model for RC columns and wall", *Matrix Analysis of Structural Dynamics-Application and Earthquake Engineering*, Marcel Dekker, Inc., New York, 967-977.
- Chopra, A.K. (1995), *Dynamics of Structures: Theory and Applications to Earthquake Engineering*, Prentice Hall, Englewood Cliffs, New Jersey.
- Chung, Y.S., Meyer, C. and Shinozuka, M. (1998), "Modeling of concrete damage", *ACI Structural Journal*, **86**(3), 259-271.
- Clough, R.W. and Johnston, S.B. (1966), "Effect of stiffness degradation on earthquake ductility requirements", *Proc. of Japan Earthquake Engineering Symposium*, October.
- Clough, R.W. and Gidwani, J. (1976), "Reinforced concrete frame 2: Seismic testing and analytical correlation", *Earthquake Engrg. Research Center Report No. EERC 76-15*, Univ. of California, Berkeley, Calif.
- D'Ambrisi, A. and Filippou, F.C. (1997), "Correlation studies on an RC frame shaking-table specimen", *Earthq. Eng. Struct. Dyn.*, **26**, 1021-1040.
- Dowell, R.K., Seible, F. and Wilson, E.L. (1998), "Pivot hysteresis model for reinforced concrete members", *ACI Structural Journal*, **95**(5), 607-617.
- Fang, I.K., Yen, S.T., Wang, C.S. and Hong, K.L. (1993), "Cyclic behavior of moderately deep HSC beam", *J. Struct. Eng.*, ASCE, **119**(9), 2537-2592.
- FEMA-273 (1997), *FEMA, NEHRP Guidelines for the Seismic Rehabilitation of Buildings*, Federal Emergency Management Agency, Washington, D.C.
- Harajli, M.H. and Mukaddam, M.A. (1988), "Slip of steel bars in concrete joints under cyclic loading", *J. Struct. Eng.*, ASCE, **114**(9), 2017-2039.
- Kwak, H.G. and Filippou, F.C. (1990), "Finite element analysis of reinforced concrete structures under monotonic loads", *Report No. UCB/SEMM-90/14*, Structural Engineering Mechanics and Materials, University of California, Berkeley.
- Kwak, H.G. and Kim, J.E. (1998), "Material nonlinear analysis of RC beams based on moment-curvature relations", *Journal of the Computational Structural Engineering Institute of Korea*, **11**(4), 233-245.
- Kwak, H.G. and Kim, S.P. (2001), "Bond-slip behavior under monotonic uniaxial loads", *Eng. Struct.*, **23**(3), 298-309.
- Kwak, H.G. and Kim, S.P. (2002), "Nonlinear analysis of RC beams based on moment-curvature relation", *Comput. Struct.*, **80**, 615-628.
- Kwak, H.G. and Kim, D.Y. (2001), "Nonlinear analysis of RC shear walls considering tension-stiffening effect", *Comput. Struct.*, **79**(5), 499-517.
- Low, S.S. and Moehle, J.P. (1987), "Experimental study of reinforced concrete columns subjected to multi-axial cyclic loading", *Earthquake Engrg. Research Center Report No. EERC 87-14*, Univ. of California, Berkeley, Calif.
- Ma, S.M., Bertero, V.V. and Popov, E.P. (1976), "Experimental and analytical studies on the hysteretic behavior of reinforced concrete rectangular and T-beam", *Earthquake Engrg. Research Center Report No. EERC 76-2*, Univ. of California, Berkeley, Calif.
- Menegotto, M. and Pinto, P.E. (1973), "Method of analysis for cyclically loaded reinforced concrete plane frame including changes in geometry and nonelastic behavior of elements under combined normal force and bending", *Proceedings of IABSE Symposium on "Resistance and ultimate Deformability of Structures Acted on by Well Defined Repeated Loads"*, Lisbon.
- Mo, Y.L. (1994), "Dynamic behavior of concrete structures", *Developments in Civil Engineering*, **44**.
- Monti, G., Filippou, F.C. and Spacone, E. (1997), "Analysis of hysteretic behavior of anchored reinforcing bars", *ACI Structural Journal*, **94**(2), 248-261.

- Oh, B.H. (1992), "Flexural analysis of reinforced concrete beams containing steel fibers", *J. Struct. Eng.*, ASCE, **118**(10), 2821-2836.
- Owen, D.R.J. and Hinton, E. (1980), *Finite Elements in Plasticity*, Pineridge Press Limited.
- Park, R., Kent, D.C. and Sampton, R.A. (1972), "Reinforced concrete members with cyclic loading", *J. of the Struct. Div.*, ASCE, **98**(7), 1341-1360.
- Pinto, P.E. and Giuffre', A. (1970), "Comportamento del cemento armato per sollecitazioni cicliche di forte intensita", *Giornale del Genio Civile*, **5**.
- Popov, E.P., Bertero, V.V. and Krawinkler, H. (1972), "Cyclic behavior of three reinforced concrete flexural members with high shear", *Earthquake Engrg. Research Center Report No. EERC 72-5*, Univ. of California, Berkeley, Calif.
- Roufaiel, M.S.L. and Meyer, C. (1987), "Analytical modeling of hysteretic behavior of reinforced concrete frame", *J. Struct. Eng.*, **113**(3), 429-444.
- Saatcioglu, M., Alsiwat, J.M. and Ozcebe, G. (1992), "Hysteretic behavior of anchorage slip in RC members", *J. Struct. Eng.*, ASCE, **118**(9), 2439-2458.
- Sawyer, H.A. (1964), "Design of concrete frames for two failure states", *Proc. of the Int. Sym. on the Flexural Mechanics of Reinforced Concrete*, ASCE-ACI, Miami, November, 405-431.
- Seaoc (1999), *Tentative Guidelines for Performance Based Seismic Engineering*, SEAOC Blue Book, Structural Engineers Association of California.
- Spadea, G. and Bencardino, F. (1997), "Behavior of fiber-reinforced concrete beams under cyclic loading", *J. Struct. Eng.*, ASCE, **123**(5), 660-668.
- Takeda, T., Sozen, M.A. and Nielsen, N.N. (1970), "Reinforced concrete response to simulated earthquake", *J. of the Struct. Div.*, ASCE, **96**(12).
- Taucer, T., Spacone, E. and Filippou, F.C. (1991), "A fiber beam-column element for seismic response analysis of reinforced concrete structures", *Earthquake Engrg. Research Center Report No. EERC 91-17*, Univ. of California, Berkeley, Calif.
- Watson, S. and Park, R. (1994), "Simulated seismic load tests on reinforced concrete column", *J. Struct. Eng.*, ASCE, **120**(6), 1825-1849.
- Wight, J.K. and Sozen, M.A. (1975), "Strength decay of RC columns under shear reversals", *J. of the Struct. Div.*, ASCE, **101**(5), 1053-1065.